Distribution and features of landslides in the Tianshui Basin, Northwest China

ZHANG Ze-lin[1]* https://orcid.org/0000-0001-8180-0787; ✉e-mail: 249133236@qq.com

WANG Tao[2] https://orcid.org/0000-0003-0075-3398; e-mail: 58227005@qq.com

WU Shu-ren[2] https://orcid.org/0000-0001-7910-8791; e-mail: 18601257415@163.com

*Corresponding author

1 China Agricultural University, Beijing 100083, China

2 Chinese Academy of Geological Sciences Institute of Geomechanics, Beijing 100081, China

Citation: Zhang ZL, Wang T, Wu SR (2020) Distribution and features of landslides in the Tianshui Basin, Northwest China. Journal of Mountain Science 17(3). https://doi.org/10.1007/s11629-019-5595-4

Abstract: Landslides in Tianshui Basin, Gansu Province, Northwest China, severely affect the local population and the economy; therefore, understanding their evolution and kinematics is of great interest for landslide risk assessment and prevention. However, there is no unified classification standard for the types of loess landslides in Tianshui. In this study, we explored the landslide distribution and failure characteristics by means of field investigation, remote sensing interpretation, geological mapping, drilling exploration and shear-wave velocity tests, and established a database of Tianshui landslides. Our analysis shows that shear zones in mudstone usually develop in weak intercalated layers. Landslides occur mainly along the West Qinling faults on slopes with gradients of 10° to 25° and on southeast- and southwest-facing slopes. These landslides were classified into five types: loess landslides, loess–mudstone interface landslides, loess flow-slides, loess–mudstone plane landslides and loess–mudstone cutting landslides. We discussed the evolution and failure process of each landslide type and analyzed the formation mechanism and motion characteristics of large-scale landslides. The analysis results show that the landslides in the study area are characterized by a gentle slope, long runout and high risk. The relationship between the runout L and the vertical drop H of the large-scale landslides in the study area is $L > 4H$. There are good correlations between the equivalent friction coefficient of large-scale landslides and their maximum height, runout, area and volume. The sliding zone of large-scale landslides often develops in the bedrock contact zone or in a weak interlayer within mudstone. From microstructure analysis, undisturbed mudstone consists mainly of small aggregates with dispersed inter-aggregate pores, whereas sheared clay has a more homogeneous structure. Linear striations are well developed on shear surfaces, and the clay pores in those surfaces have a more uniform distribution than those in undisturbed clay.

Keywords: Loess Plateau; Landslide distribution; large-scale landslide; landslide types; slide distance; Qinling fault

Introduction

Landslide was often neglected as a geomorphic process in the earliest models of landform evolution. While there has been a growing acknowledgement of landslide as a hillslope process capable of performing significant

erosion and transportation, it has received only sparse recognition as a formative process in its own right (Crozier 2010). Present research is focused on local site specific investigations or regional analysis. Observation methods range from the use of geotechnical in-situ measurement devices to spatial analysis techniques like GIS, including remote sensing tools.

A landslide is a complex natural phenomenon which can develop into a serious natural disaster (Malamud et al. 2004). The morphology of the Loess Plateau in China is affected by topography, seismic activity, fault structure, bedrock structure and the overlying loess (Derbyshire 2001). Loess landslides have different features and different distribution characteristics in different regions on the Loess Plateau. The landslides in Heifangtai terrace were induced by irrigation (Peng et al. 2018; Zhang and Wang 2018). On December 16, 1920, the Ningxia Haiyuan M_S 8.5 earthquake triggered 657 large-scale loess landslides causing heavy casualties (Zhuang et al. 2018). Loess landslides can also be induced by rainfall and construction work.

A landslide database is a detailed record of the distribution and characteristics of past landslides (Rosi et al. 2017). A landslide database and inventory can be utilized to record the scale of landslides, provide a basis for landslide risk assessment, study the morphological and geological characteristics of landslide types and their distribution, and investigate landslide evolution and failure mechanisms (Duman et al. 2005; Van Westen et al. 2006; Parker et al. 2011; Rosi et al. 2017).

To establish a landslide database and inventory, data are collected by field mapping, remote sensing, high-resolution digital elevation models (DEMs), and synthetic aperture radar (SAR) images (Yang and Chen 2010; Qu et al. 2017; Sato et al. 2017; Spreafico et al. 2018; Huang et al. 2019). A landslide inventory records the size of landslides, their type, frequency, state, failure factors and other details, providing a basis for investigation of landslide evolution and mechanism.

Varnes (1978) presented a detailed landslide classification report which was updated in 2014 by Hungr et al.. Meng and Derbyshire (1998) classified loess landslides as bedrock contact landslides, paleosol contact landslides, multi-layered landslides, loess landslides, terrace landslides and Tan-ta landsides. Wu and Wang (2006) classified loess landslides as interface landslides, plane landslides and cutting landslides. Loess landslides are often considered to be the sliding or flow of a single land mass. However, in a complex geological environment, the sliding mass can be subdivided, resulting in various types of loess landslides depending on the geological environment.

Geological survey results show that in the Tianshui area of Gansu Province, China, the bedrock mudstone and overlying loess strata were affected by strong historical earthquakes. Landslides are densely distributed, with large-scale landslides occurring mainly on river erosion shores and in valleys. Many of these landslides have high mobility, with a long runout and high sliding velocity. On June 19, 1718, an earthquake (M_S = 7.5) occurred in Tongwei, Gansu Province. The earthquake triggered more than 300 large-scale landslides in the Ganggu and Tongwei areas (the meizoseismal area), causing more than 30,000 deaths (Wu and Wang 2006; Sun et al. 2017). Many major earthquakes have occurred on the Loess Plateau, for example the Gangu West M_S 7.0 earthquake in 143 AD, the Tianshui M_S 7.0 earthquake in 734 AD, and the Tianshui South M_S 8.0 earthquake in 1654 (Meng and Zhang 1989; Chen et al. 2005). Gansu is one of the regions with the strongest tectonic activity in China and is very prone to geological disasters. Most of the historic seismic geological hazard sites are still relatively unaltered because of the lack of human activities, providing unique conditions for exploring the causes of seismically induced geological hazards and their mechanisms in their natural setting.

In this paper we present a dataset of the distribution and typical features of landslides that occurred in the Tianshui area, China between 2013 and 2018. The database, containing 3856 landslides, was acquired through field investigation and QuickBird satellite images taken by China. And european Remote Sensing (ERS)1-2 and Envisat images was used as a complement. The primary objectives are to study the distribution characteristic of these landslides as a supplementary dataset, to classify the landslides that occur in loess areas and to analyze the morphological and geological features of these landslides. Typical cases in the study area are

presented and their geometric features, slope structures, slip surface and formation mechanisms are analyzed. Our results can provide an engineering basis for early geo-hazard identification and prevention, and guidelines for further hazard and risk analysis in the Tianshui area.

1 Study Area

1.1 Geologic setting

The Tianshui Basin is situated in the Tianshui area, Gansu Province, China, and is part of the Loess Plateau (Figure 1). The West Qinling fault belt is a major regional fault; the northern edge of the fault has a strong effect on the Tianshui Basin (Han et al. 2001; Li et al. 2016). The fault lies along the south bank of the Weihe River and runs in a WNW direction. The flat area dips SW with a dip angle of 70°–75° and extends for approximately 80 km. The geomorphic features on the southern side of the fault differ from those on the northern side, with low mountain valleys to the south and medium–high mountains to the north. According to historical records (AD 128–1979), earthquakes have occurred frequently in the Tianshui area, including 20 earthquakes of M_S 6.0 or higher, the

largest being a M_S 8.0 event that triggered many landslides (Wang et al. 2018; Liu et al. 2007). The basic seismic acceleration in the Tianshui area (exceedance probability 10% in 50 years) is 0.2–0.3 g.

The bedrock in the Tianshui Basin is composed of Proterozoic gneiss, Triassic sedimentary and metamorphic rocks, and Devonian and Cretaceous sandstone. The main bedrock is Neogene mudstone deposited in rivers and inland lakes, red mudstone intercalated with sand conglomerate and gray-white and gray-green clay rocks, with a total thickness of more than 1000 m. The bedrock and the basin are covered with Quaternary deposits such as loess, landslide deposits, alluvial and diluvium deposits. The loess at the top of the sequence, which is 10−30 m thick, has low stability and can easily collapse under rainfall and earthquake conditions. The underlying mudstone has low permeability and is easily weathered, forming a weak interlayer. Rotational–translational landslides are concentrated at the northeast margin of the Qinghai–Tibet Plateau (Xin et al. 2018).

1.2 Engineering geological conditions for landslides

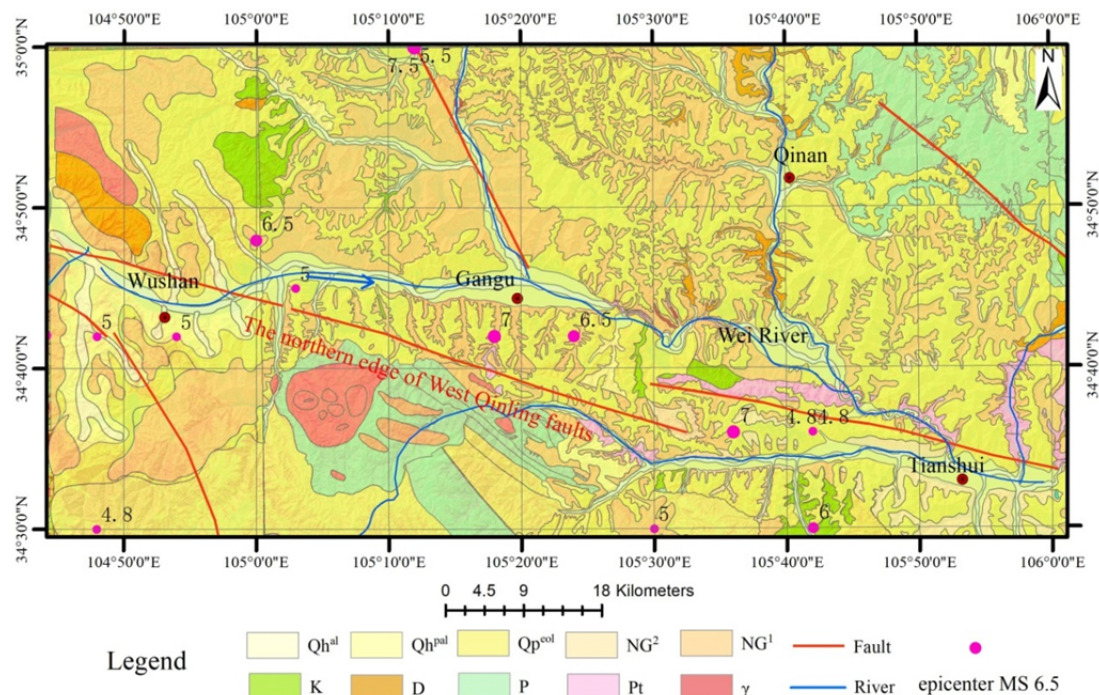The mudstone has low permeability and is

Figure 1 Location and Geological settings of Tianshui Basin.

highly sensitive to water from rainfall (Sun et al. 2017; Peng et al. 2015); thus, the rock will expand and soften considerably after exposure to water. The stability of a slope rock mass is controlled by different structural planes, especially weak intercalated layers in mudstone. The creep behavior of the soft rock and weak intercalated layers is significant. The bedrock of the slope is Neogene mudstone covered by Pleistocene loess. The majority of landslides occur in the loess and
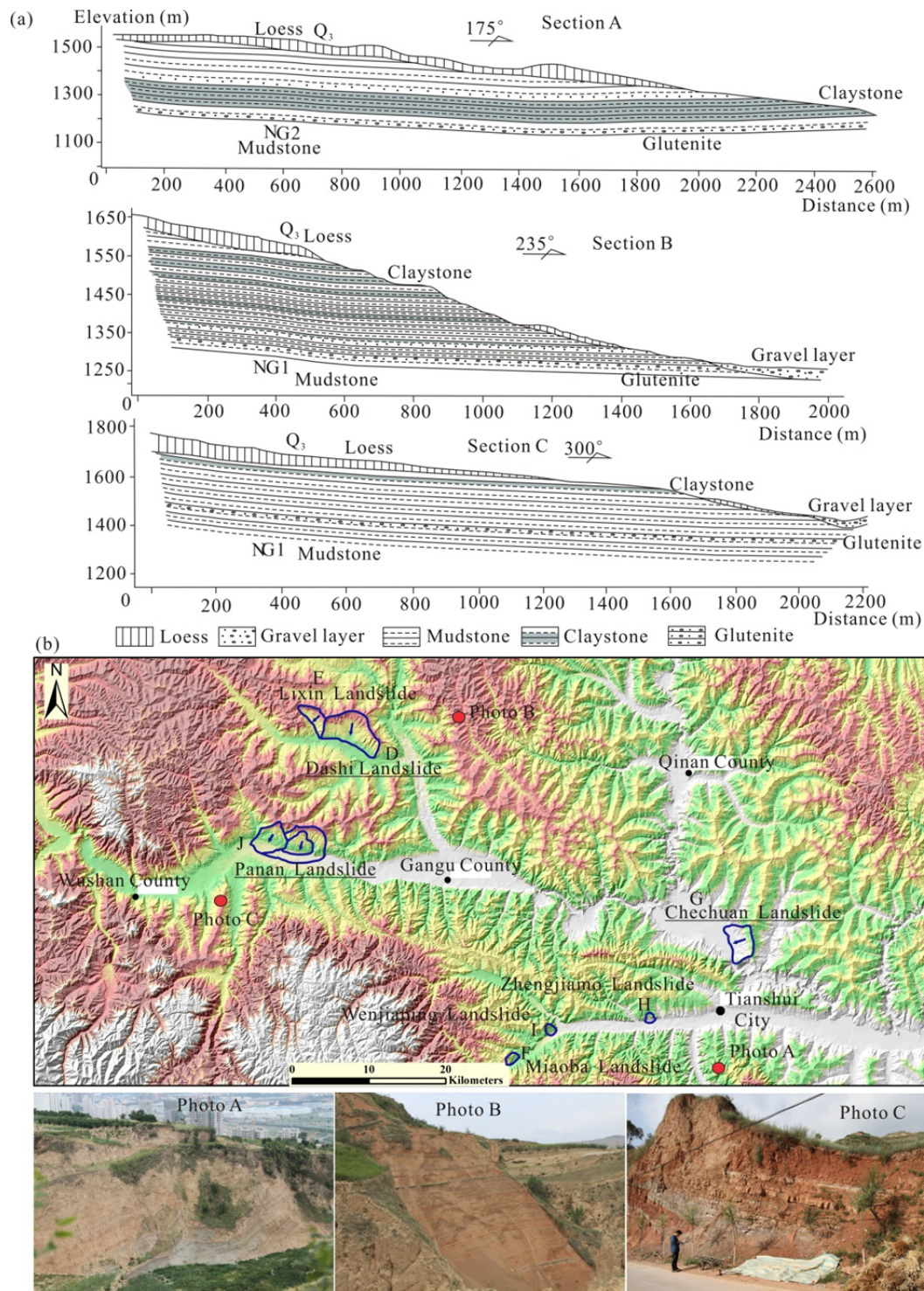

Figure 2 The slope structure in Tianshui Basin. (a) Three representative types of slope section A, the slope in Tianshui City; section B, the slope in Gangu County; and section C, the slope in Wushan County. (b) The slope distribution map and the slope photos A, B and C.

mudstone layers. The red mudstone is composed mainly of clay, with a small amount of sandy silt (Appendix 1). The lithology of the slope in the study area is mostly interbedded soft and hard rock, with an overlying layer (10–30 m thick) of loess. The soft rock (weathered mudstone) contains a weak intercalated layer. The mudstone is rich in kaolinite, illite and montmorillonite. The structural characteristics of the slope are shown in Figure 2. The Neogene rocks, near the horizontal sedimentary strata, contain an upper mudstone unit (NG2) and a lower mudstone unit (NG1). The bottom of the upper unit (NG2) is mainly gray and light gray-green mudstone or claystone, with small amounts of red claystone. The top part of NG2 is mainly red claystone, with a thin interlayer of white or gray-green mudstone. The lower segment (NG1) is mainly red argillaceous rock with a small amount of claystone, with layers of intercalated conglomerate and sand gravel with poor diagenesis.

During field investigations, three representative types of slope were discovered (Figure 2): section A, the slope in Tianshui City (photo A); section B, the slope in Gangu County (photo B); and section C, the slope in Wushan County (photo C). Section A has bedrock of Neogene red mudstone. The lower bedrock contains red straticulate mudstone with a small amount of glutenite. The mudstone contains calcareous nodules and a sedimentation pattern of mud and gravel. The upper bedrock contains grayish-white and greenish-gray argillaceous shales, claystone and glutenite. The upper layer of the slope is a 10–30-m-thick layer of loess. The rock strata at the foot of the slope crop out in the opposite direction to the dip.

Section B has bedrock of Neogene red mudstone with horizontal bedding and poor diagenesis with a small amount of glutenite and some gravel lenses. The lower bedrock is red sandy claystone with a small amount of glutenite. The gravel size becomes gradually finer from the bottom to the top of the bedrock. The slope is covered with a 2–5-m-thick layer of loess.

Section C has bedrock of Neogene red mudstone and claystone with a small amount of glutenite, with poor diagenesis. The upper layer of the slope is straticulate loess.

These mudstone strata are horizontally bedded (Figure 2), and occur widely in the valley areas.

These mudstones represent risks to slope stability because of the presence of faults and weak intercalated layers.

2 Methods

The landslide data were acquired by field investigation and interpretation of remote sensing images. The backwall of a landslide has notable armchair-shaped features that can be identified during image interpretation (QuickBird satellite image, resolution 0.61 m). The method of remote sensing image interpretation is based on visual interpretation involving image recognition, image measurement and image analysis. Approximately 80% of the landslides were visited during the field investigation. During the field survey, landslide data were collected using handheld GPS and laser scanning units. Measurements included the landslide location and its width L and height H. Additionally, borehole data were acquired at some large-scale landslides. Volumes are much more difficult to measure than areas, as areas can be obtained from aerial photographs, but volumes usually cannot. The pre-landslide DEM dataset was bought from the State Bureau of Surveying and Mapping (1:10,000 DEM, 5-m spatial resolution). Some quite ancient landslides are on a usually large scale. We carried out detailed field investigations and drilling explorations. We determined the depths of sliding surfaces on the basis of information from drill holes. From these measurements, landslide area and volume were estimated. Landslide data such as area and volume can also be derived from DEM data using ArcGIS 10.0 software to interpret the images. Landslide volumes were estimated mainly based on the pre-/post-DEM calculation. Core samples from boreholes provided borehole logs and the engineering geologic profiles of the landslides were drawn using Corel Draw. We conducted shear-wave velocity tests on the core samples following the standards of the China Method of Soil Test (GBT50123–1999). Finally, to identify microstructural features in large-scale landslides, scanning electron microscopy (SEM) was used to evaluate the characteristics and performance of undisturbed mudstone and sheared clay from the sliding surface.

3 Landslides Types and Features

3.1 Landslide distribution

The establishment of a landslide database can help with research on landslides at various scales, and provide a basis for assessing landslide-prone areas and evaluating the risks. Our research was carried out in a heavily populated, landslide-prone area.

The landslide database contains 3856 recorded landslides (Figure 3a). The landslides in the Tianshui Basin are mostly loess–mudstone landslides triggered by rainfall and earthquakes. Preliminary results showed that 55% of the landslides (mainly small and medium-sized landslides) were caused by rainfall, 45% of the landslides (mainly medium-sized and large landslides) were earthquake-caused, and 35% of the landslides were caused by both rainfall and
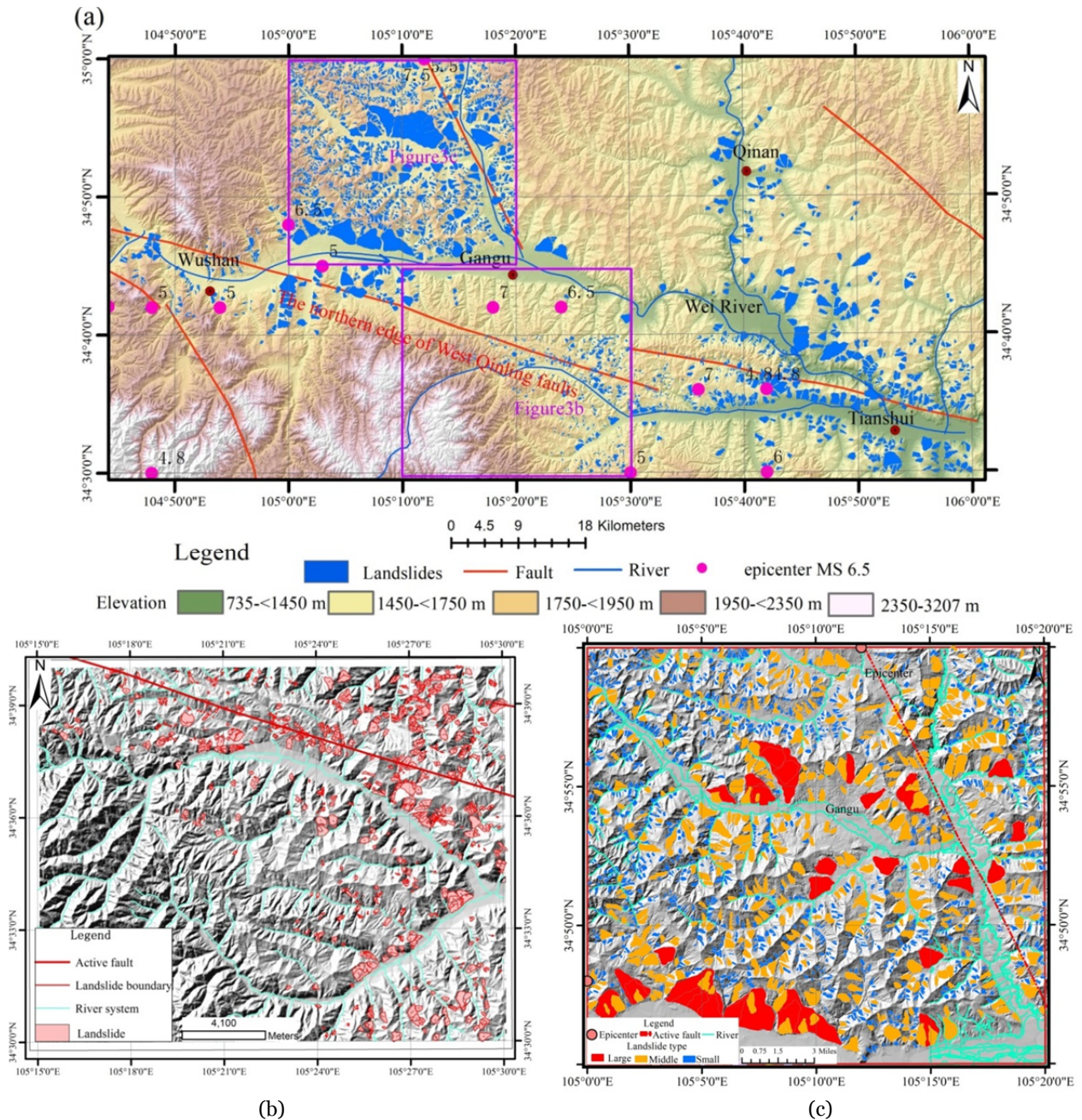

Figure 3 (a) Landslide distribution map in Tianshui area, (b) Landslide distribution map in the west of Tianshui City, and (c) Landslide distribution map of Gangu town.

earthquake. Figure 3b shows some of the database landslides, located west of Tianshui City. The landslide elements are mapped in detail. Another area west of Tianshui City is shown in Figure 3c; this area covers ~845 km2 and contains the landslides caused by the 1718 Tongwei earthquake

(Sun et al. 2017). The area covered by landslides in Figure 3a is approximately 227 km², accounting for 26.86% of the total map area. A strong earthquake struck the town of Tongwei in Gansu Province, China on June 19, 1718. Historic records indicate that the landslides triggered by the earthquake
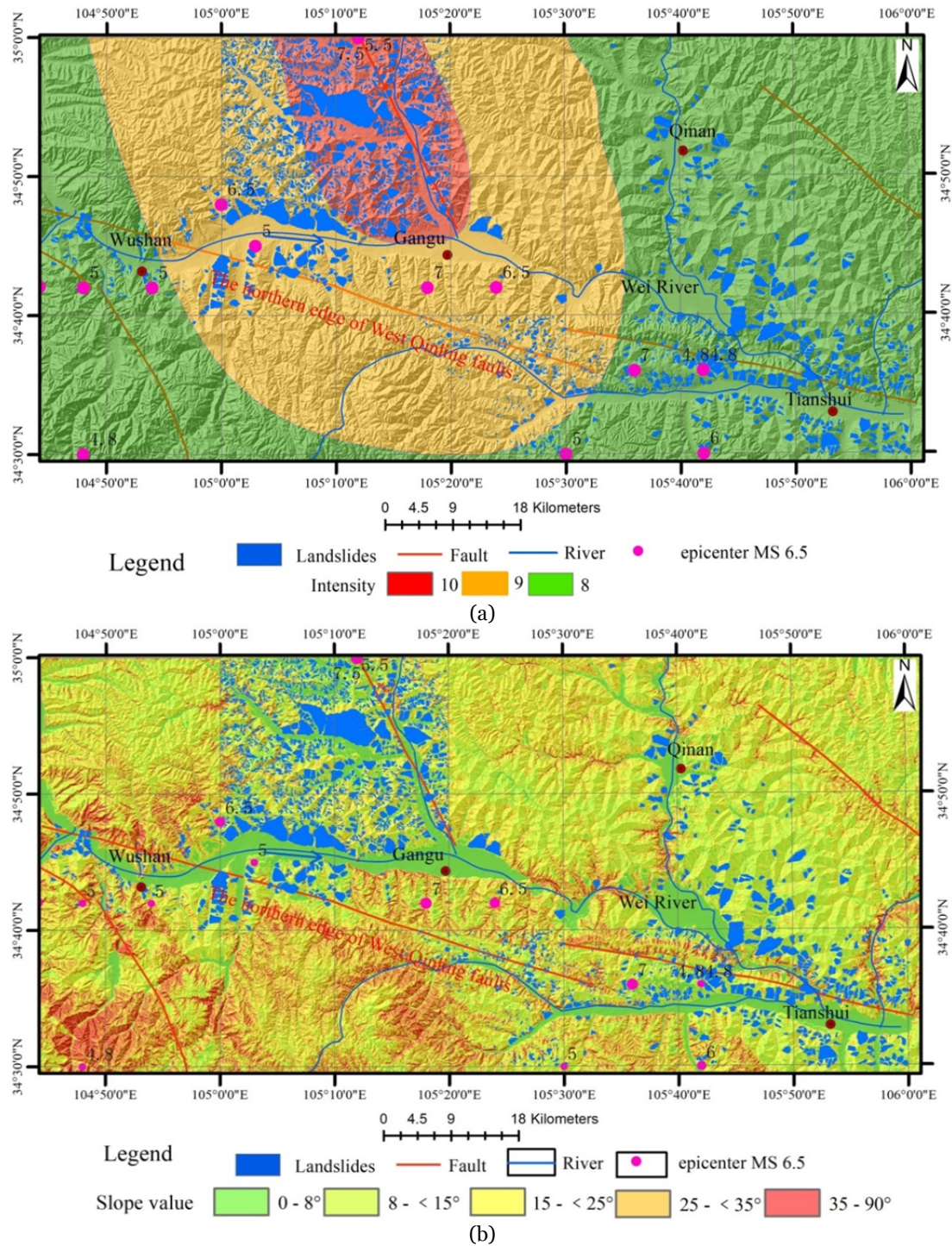

(a)

(b)

Figure 4 Landslide distribution in the area affected by the 1718 Tongwei Earthquake (a) Intensity; (b) Mountain slope angle display.

caused tens of thousands of deaths (Da et al. 2017). Many landslides occurred throughout the high-seismic-intensity area. Almost 300 years after the Tongwei earthquake, although some landslides have been eroded by weathering, landslide evidence can still be found in the region. By means of oral history passed down through generations, local people have retained the history of the earthquake. The loess and weak mudstone are sensitive to water; therefore, rainfall and earthquakes have greatly influenced the geomorphology of the region. Other strong earthquakes have occurred in and near the area (China Seismological Bureau 1980).

The landslides are distributed mainly along the West Qinling faults (Figure 4a). Some of these landslides were caused by earthquakes (Li et al. 2009; Harp and Jibson 1996; Lin and Tung 2004; Owen et al. 2008; Sato and Harp 2009) that were generated by fault motion. The landslide database includes the orientations and gradients of the landslides; the angles of slopes in the region are illustrated in Figure 4b. Statistical analysis indicates that the landslides occur mainly on slopes with gradients ranging from 10° to 25° and on southeast- and southwest-facing slopes (Figure 5).

The geomorphology of the landslide area is relatively gentle. The gentle geomorphology may result from rainfall- and earthquake-induced landslides or long-term geological erosion. The northern West Qinling faults are strike-slip faults with right-lateral motion. In the area of dense landslide occurrence, landslide directions are generally orthogonal to the fault direction.

In geomorphological terms, landslides are mostly located on both sides of loess ridges. Landslides readily occur under conditions of long-term erosion and earthquakes. Since the late Cenozoic, the loess plateau has experienced intermittent uplift. Controlled by the base level of erosion, the plateau has experienced strong erosive cutting. With the development of river systems, ravines and valleys, the terrain has become fragmented, which provides the necessary gravitational conditions and activity space for loess landslides. According to Davis' erosion-cycle theory, loess landforms go through an evolutionary sequence of loess tableland → loess ridge → loess hill (Derbyshire 2001). Large-scale loess landslide landforms possess a large, steep back wall containing several small gullies. It also forms a broad and gentle platform on the sliding body.

3.2 Landslide type

According to the landslide database, 61.4% of the landslides are loess–mudstone plane/cutting landslides, 63.3% have volumes of more than 10^5 m³, and 68.4% are less than 10 m deep (Table 1). The loess landslides in the Chinese Loess Plateau can be classified on the basis of their features. Peng et al. (2018) classified the landslides of loess-related slope failures in Heifangtai and the Loess Plateau of China. Following the landslide classification system of Varnes (1978) and Hungr et al. (2014), who classified landslides on the basis of their characteristics and their sliding surfaces, we divided the landslides in our study area into five types: loess landslides, loess–mudstone interface landslides, loess flow-slides, loess–mudstone plane
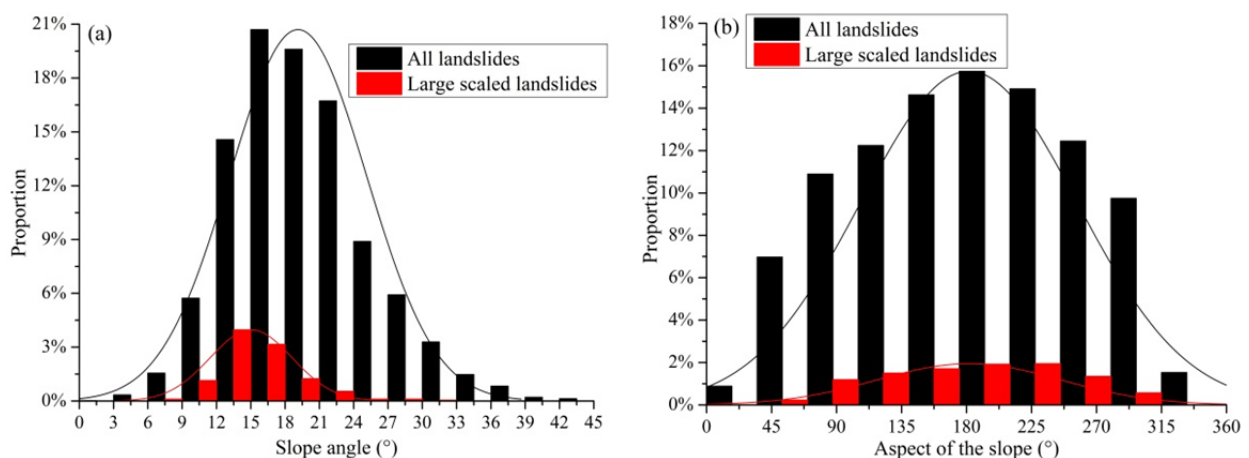

Figure 5 Landslide statistics about (a) the slope angle and (b) slope aspect.
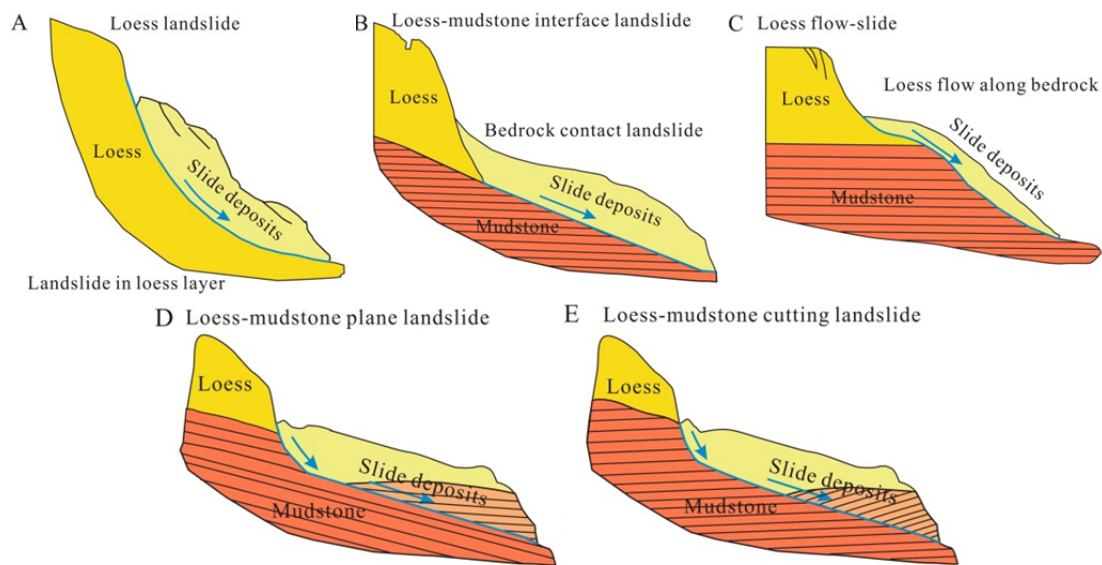
Figure 6 Loess landslides types in Tianshui Basin. (A, loess landslides; B, loess-mudstone interface landslide; C, loess flow-slide; D, loess-mudstone plane landslides; and E, loess-mudstone cutting landslides).

Table 1 A brief table of landslide classification in the study area.

Classification factors	Landslide type	Description	Landslide numbers	Proportion (%)
Landslide volume	Small-sized	$<10^5$ m³	1417	36.7
	Medium-sized	10^5 m³—10^6 m³	2035	52.8
	Large-sized	$>10^6$ m³	403	10.5
Landslide thickness	Superficial type	<10 m	2638	68.4
	Medial type	10 m—25 m	1052	27.3
	Deep-seated	>25 m	166	4.3
Sliding Surface feature	Loess landslide	Landslide in loess layer	593	15.4
	Loess-mudstone interface landslide	Bedrock contact landslide or Slid surface in bedrock	746	19.3
	Loess flow-slide	Loess slide and then flow along the bedrock	150	3.9
	Loess-mudstone plane/cutting landslide	Landslide in mudstone and loess (mixed)	2367	61.4

landslides and loess–mudstone cutting landslides (Figure 6). These landslide types are described below.

1. Loess landslide (Figure 6A): for this landslide type, the failure surface is in the loess layer, and the landslide occurs entirely in the loess. The sliding surface suggests rotational sliding, and cracks in the loess influence the slope stability. This kind of landslide often exhibits small-scale failure and short-distance sliding (runout). Human engineering activities, rainfall and earthquakes are the main triggers of this type of landslide.

2. Loess–mudstone interface landslide (Figure 6B): for this type of landslide, the failure surface lies along the interface between the bedrock and the overlying loess. Failure occurs as the loess slides along the bedrock; the sliding surface suggests translational sliding. This kind of landslide often presents as a medium-scale failure with a long sliding distance (runout). Rainfall and earthquakes are the main triggers of this type of landslide.

3. Loess flow-slide (Figure 6C): for this landslide type, the sliding surface is along the bedrock. Failure occurs as the loess flows along the bedrock, implying flowing and sliding motion. This kind of landslide often manifests as a thin layer of flowing–sliding loess with a long runout distance. Rainfall is the main trigger of this type of landslide.

4. Loess–mudstone plane landslide (Figure 6D): in this type of landslide, cracks develop in the loess layer and extend down along the bedding plane of the bedrock, causing failure. Failure occurs in both the loess and the bedrock, and the slide

surface suggests initial rotation followed by translational sliding. This kind of landslide often presents as deep-seated large-scale failure with a long sliding distance (runout). Rainfall and earthquakes are the main triggers of this type of landslide.

5. Loess–mudstone cutting landslide (Figure 6E); in this type of landslide, cracks develop in the loess layer and extend downward, cutting into the bedrock. Failure occurs in both the loess and the bedrock, and the sliding surface suggests roto-translational sliding. This kind of landslide often presents as deep-seated large-scale failure with a long sliding distance (runout). Earthquakes and rainfall are the main triggers of this type of landslide.

3.2.1 Loess landslide

A total of 593 landslides in the study area are loess landslides, in which the failure surface occurs in the loess. A typical example is the Tool Factory landslide located in Tianshui City (Figure 7). The main sliding direction of the landslide is 210° and the average slope gradient is 16°. The landslide has a length of 350 m, a width of 280 m, an average thickness of ~20 m, and a volume of ~1.4×10^6 m³. Field studies of the sliding body indicate that the slide deposits are loess and the sliding surface is cambered. The bedrock exhibits horizontal stratification. The landslide is medium-sized with a

relatively short runout. This kind of landslide often occurs after rainfall where construction or infrastructure work has cut into the slope and rainwater has reduced the strength of the loess.

The failure pattern of loess landslides is presented in Figure 7c. In stage 1, cracks and joints develop at the slope crest, caused by toe excavation and rainfall. In stage 2, the cracks at the crest gradually extend downward and a concave sliding surface is formed. Stage 3 is the failure stage, in which the unstable block slides along the concave failure surface. This process is common in landslides in the Chinese Loess Plateau with small-to medium-sized failure.

3.2.2 Loess-mudstone interface landslide

A total of 746 landslides in the study area are loess–mudstone interface landslides, in which failure occurs in the loess layer that slides along the bedrock–loess interface. A typical example is the Malan village landslide in Tianshui City (Figure 8). The main sliding direction of the landslide is 217° and the average slope gradient is 11°. The landslide has a length of 2200 m, a width of 1000 m, an average thickness of approximately 30 m, and a volume of approximately 33×10^6 m³. Field surveys indicate that the slide deposits are loess and the sliding surface is translational. The bedding slope is at the top of the bedrock, and the landslide is large to medium in size, with a long runout
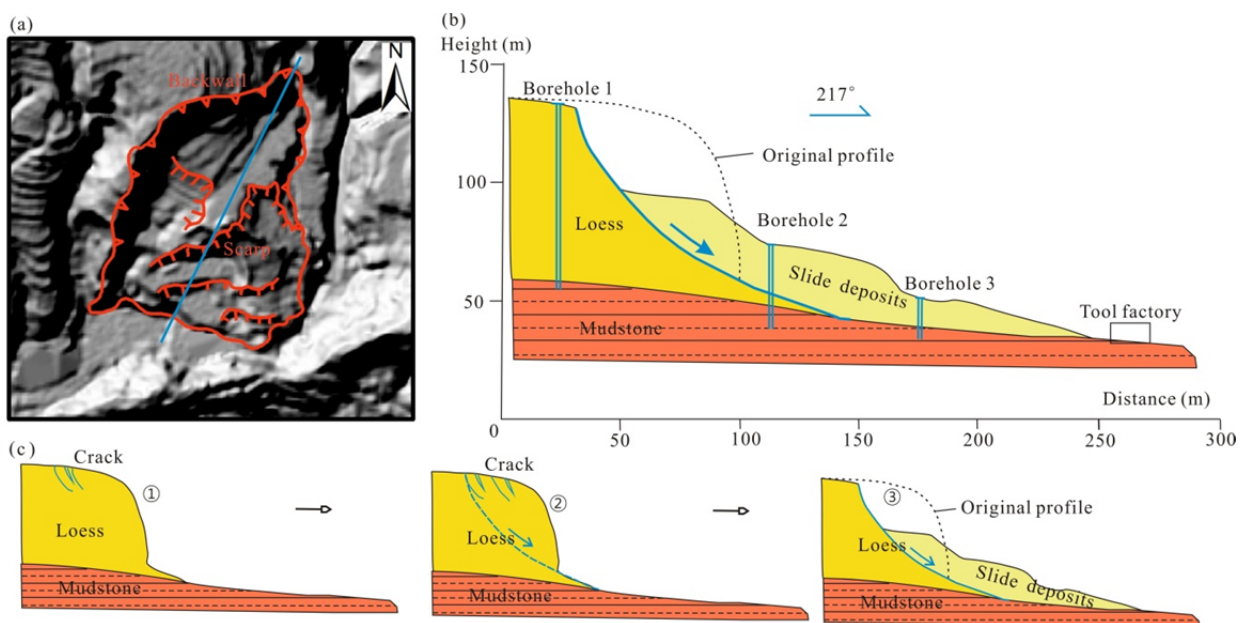

Figure 7 A typical rotational loess landslide. (a) planar map; (b) profile map; (c) failure pattern.

distance of several kilometers, based on our database. Documents indicate that the runout distance of large-scale landslides is several kilometers or more (Crandell et al. 1984; Evans et al. 1984; Wang et al. 2002).

This kind of landslide is often triggered by rainfall and earthquakes. Because mudstone has low permeability, moisture accumulates at the sliding surface, greatly reducing the shear strength. This type of landslide is common in strata with gently inclined bedding.

The failure pattern of a loess–mudstone interface landslide is presented in Figure 8c. In stage 1, cracks develop in the slope crest and gradually extend through the loess when rain infiltrates the slope. In stage 2, the cracks extend toward the bedrock and a translation slide surface forms along the bedrock interface. In stage 3, the cracks continue to propagate, causing deformation in the slope, and the slip mass begins to slide along the translation sliding surface. The failure is often on a large to medium scale with a long runout.

3.2.3 Loess flow-slide

A total of 150 landslides in the study area are loess flow-slides. In these landslides, failure occurs in the overlying loess, which flows along the bedrock. A typical example is the Mahuangzui
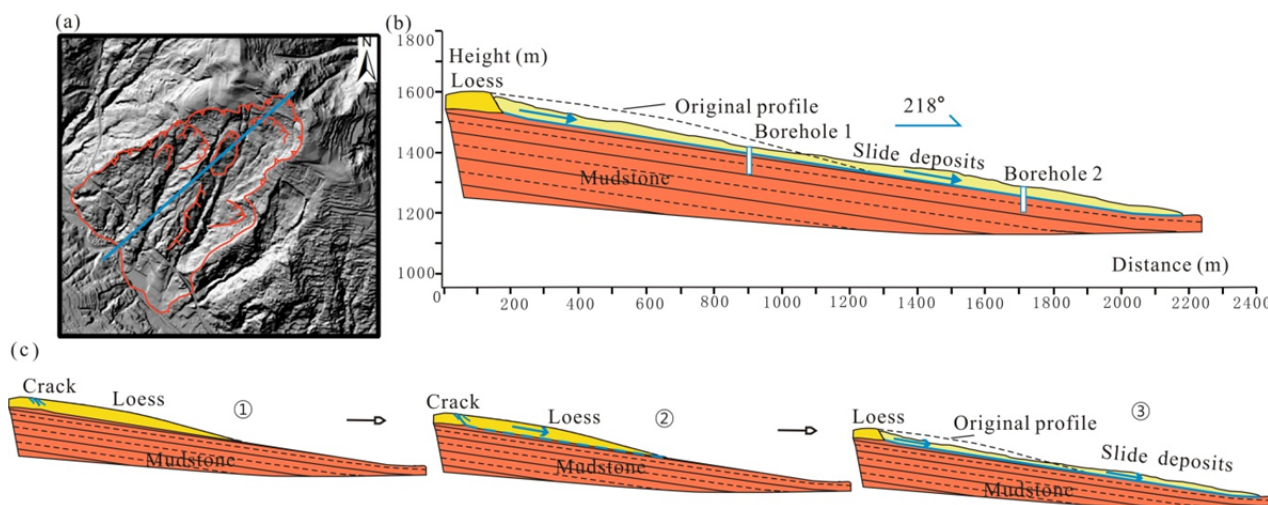

Figure 8 A typical translational loess-mudstone landslides. (a) planar map; (b) profile map; (c) failure pattern.
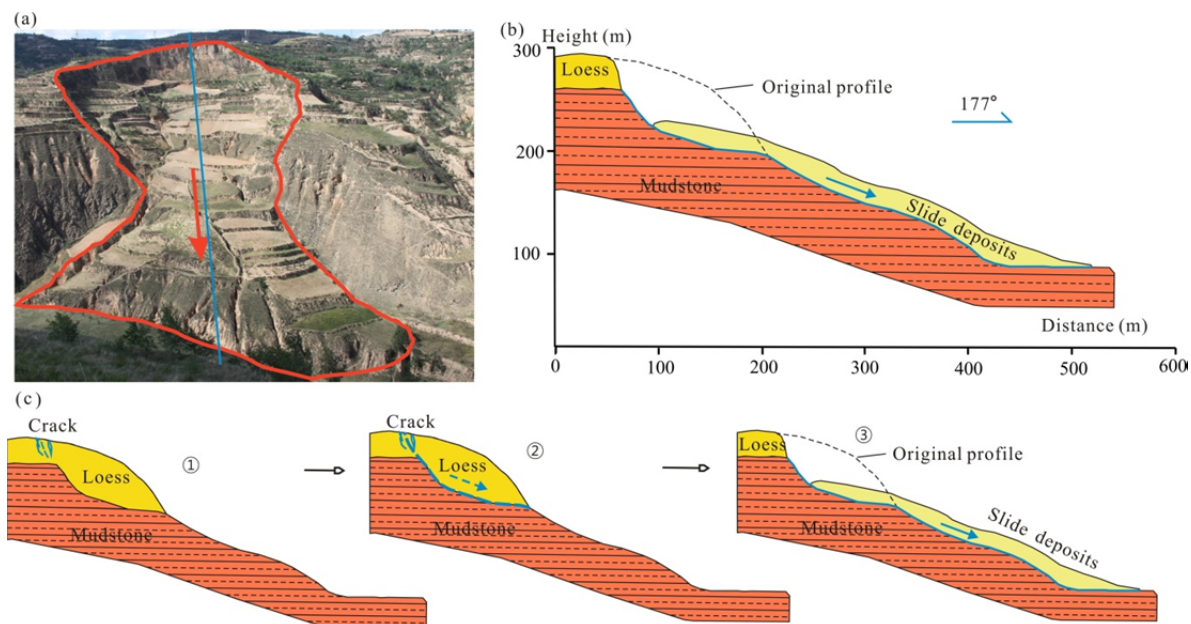

Figure 9 A typical loess flowslide. (a) geomorphologic picture; (b) profile map; (c) failure pattern.

landslide in the town of Qinan (Figure 9), which has a main sliding direction of 177° and an average slope gradient of 30°. The landslide has a length of 530 m, a width of 300 m, an average thickness of ~20 m, and a volume of ~2.5 × 10⁶ m³. Field investigations indicate that the slide deposits are loess, and the sliding surface is irregular. The bedrock is horizontally bedded mudstone, and the landslide is small and has a short runout distance. This kind of landslide is often caused by heavy rain. After the loess becomes liquefied, it flows along the bedrock. The thin layer of loess flows along the bedrock and often occurs in the tributaries of the valley.

The failure process of a rotational loess landslide is presented in Figure 9c. In stage 1, cracks develop on the slope crest, and propagate deep into the loess slope when the rain falls. In stage 2, the cracks at the crest gradually extend deep into the slope and a cambered sliding surface forms in the loess. In stage 3, failure occurs as the unstable loess flows and slides along the bedrock. The sliding surface is typically irregular with multi-staged cambers. This type of landslide is commonly found in the Chinese Loess Plateau where the loess deposits are shallow, and is normally small to medium in size.

3.2.4 Loess-mudstone plane landslide

More than 1000 landslides in the study area are loess–mudstone plane landslides, in which failure occurs in both the loess and mudstone and both slide along a bedding plane. A typical example is the Liping village landslide located in the town of Wushan (Figure 10). The main sliding direction of this landslide is 354° and the average slope gradient is 23°. The landslide has a length of 1700 m, a width of 1400 m, an average thickness of approximately 70 m, and a volume of approximately 65 × 10⁶ m³. The slide deposits are loess and mudstone, and the strata in the deposited mudstone are inverted. The sliding surface is cambered at the upper part of the slope and translational at the middle and lower parts. The sliding plane is in the bedrock and the landslide is large, with a long runout. This kind of landslide is often caused by heavy rain and earthquakes. Weak interlayers in the mudstone play a crucial role in the rock failure. When rain permeates into the weak interlayers, the shear strength decreases. The landslide often exhibits creep deformation under the forces of gravity and water. A strong earthquake can trigger a deep-seated, devastating landslide with a long runout.

The failure pattern of a loess–mudstone plane landslide is presented in Figure 10c. In stage 1, cracks develop on the slope crest, and propagate into the deep mudstone layer as the loess absorbs the rainfall. In stage 2, the cracks at the crest gradually extend deep into the slope strata, and a cambered slide surface forms in the loess. Weak interlayers are formed and the translational plane is extended. This is the creep deformation stage of landslide formation. In stage 3, failure occurs after
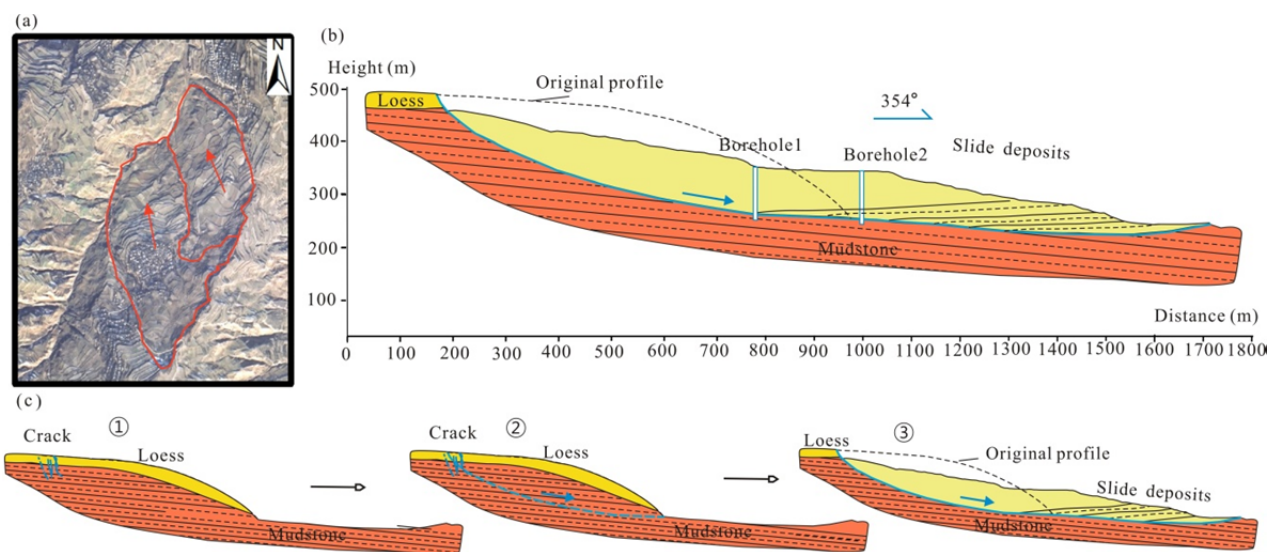

Figure 10 A typical loess-mudstone plane landslide (mixed, bedding plane landslide). (a) geomorphologic picture; (b) profile map; (c) failure pattern.

a strong earthquake and the unstable parts of the slope slide along the bedding plane. The sliding surface is often roto-translational. The deposits have a long runout and are deep-seated. Large-scale landslides of this type are common in the meizoseismal area of the Chinese Loess Plateau.

3.2.5 Loess-mudstone cutting landslide

More than 1000 landslides in the study area are loess–mudstone cutting landslides, in which failure occurs in both the loess and the mudstone and both rock masses slide along a plane that cuts through the bedrock beds. A typical example is the Wenjiaping landslide located in Tianshui City (Figure 11). Its main sliding direction is 170° and the average slope gradient is 27°. The landslide has a length of 1100 m, a width of 900 m, an average thickness of 60 m, and a volume of 30×10^6 m³. The slide deposits are loess and mudstone. As in other roto-translational landslides, the sliding surface is cambered in the upper part of the slope and a translational interface is present in the middle and lower parts. The bedrock exposure forms a slightly anti-dipping slope, and the landslide is large, with a long runout. Heavy rainfall and earthquakes are the main causes of this type of landslide. When rain permeates the cracks and interlayers, the shear strength of the mudstone decreases. The landslide shows creep deformation under gravity and water. A strong earthquake can result in a deep-seated landslide with a long runout.

The failure pattern of a loess–mudstone cutting landslide is presented in Figure 11c. In stage 1, cracks develop at the crest. In stage 2, the cracks at the crest gradually extend deep downward. A cambered slide surface forms in the loess. Weak interlayers develop in the cracked bedrock, until a continuous translational plane is formed. The slope deformation suggests the occurrence of creep in the deep-seated interlayers. In stage 3, failure occurs after a strong earthquake and the unstable parts slide along the translational plane in the bedrock. The sliding surface is roto-translational. The deposits are deep-seated over a long runout. Large-scale earthquake-induced landslides in the Chinese Loess Plateau usually belong to this category.

The primary reasons governing the development of bedding-plane landslides and cutting landslides may be as follows. For bedding-plane landslides, the upper part of the mudstone is subjected to weathering, leading to considerable formation of weak interlayers parallel to the surface. These weak layers with mild dip (10°–20°) have a significant impact on slope stability because of their unfavorable mechanical properties in terms of shear strength. In addition, changes to any type of external boundary conditions (such as earthquake and rainfall infiltration) are likely to enable kinematic feasibility (Zhang et al. 2018). For cutting landslides, the mudstone in the upper part is subjected to weathering, leading to weak interlayered layers and joints/ discontinuities. Usually, a strong earthquake can generate a rupture surface within the landslide, and the main
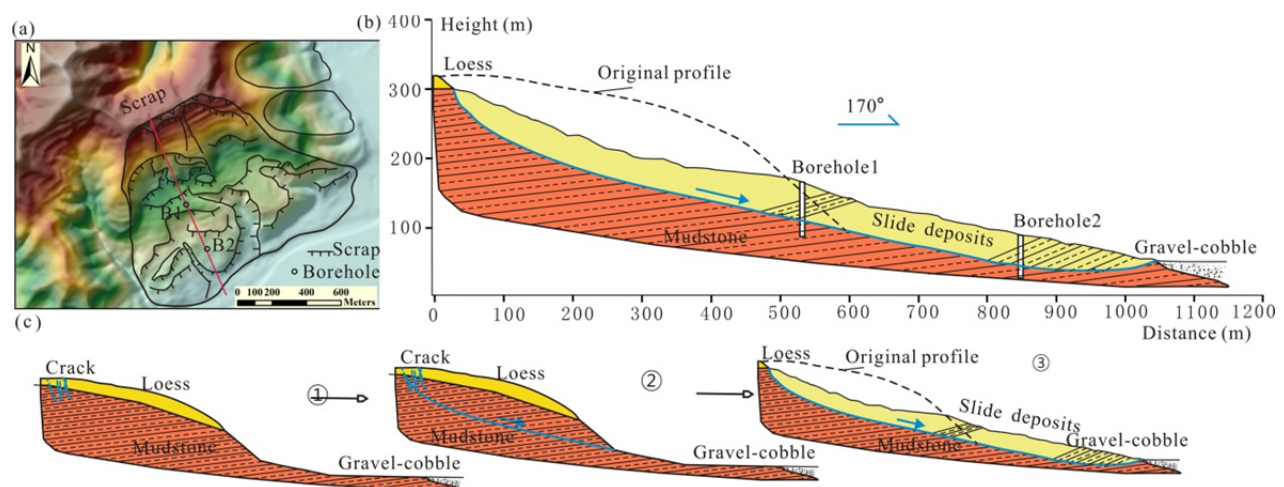

Figure 11 A typical loess-mudstone cutting landslide (mixed, cutting landslide). (a) geomorphologic picture; (b) profile map; (c) failure pattern.

scarp is steep.

3.3 Landslide motion characteristics

Strong earthquakes, engineering construction work and rainfall have triggered numerous landslides in the Loess Plateau in northwest China. The landslides in this region are characterized by a gentle slope, long runout and high failure risk. Many studies in the field of geological disasters have investigated the formation mechanism and motion characteristics of such long-range landslides. The sliding distance of a landslide is an important evaluation indicator and a direct cause of impact.

The ratio of the maximum height (H_{max}, from the crest to the toe of the landslide mass) to the maximum horizontal distance (L_{max}, from the main scarp to the toe) is often used as a parameter to describe the motion characteristics of a landslide. This characteristic parameter μ (Figure 12), also known as the apparent friction angle or the equivalent friction coefficient, is related to the kinetic energy and the dynamic friction coefficient, and can reflect the mobility of the landslide (Zhuang et al. 2018; Peng et al. 2018; Fan et al. 2018); in general, the smaller the ratio, the higher the mobility. The mobility index of the landslide is generally controlled by its volume. To study the kinematics of large-scale landslides in the study area, 403 large-scale landslides with a volume larger than 400×10^4 m³ were identified from remote-sensing images and DEM data and selected for analysis.

$$\mu = H_{max}/L_{max} \tag{1}$$

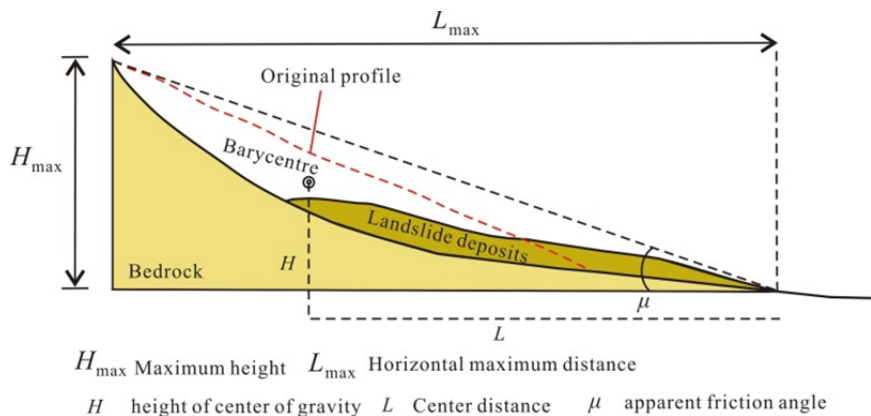From the analysis, the logarithmic relationship

between the equivalent friction coefficient of the landslide and the area and volume of the landslide was established. Figure 13a shows the statistical regression relationship between landslide L_{max} and landslide volume. The relationship can be expressed as:

$$L_{max} = \frac{891.88 - 6695.02}{1 + \left(\lg V_L / 3.81 \times 10^8 \right)^{0.87}} - 6695.02$$

$$(R^2 = 0.62884) \tag{2}$$

where V_L is the volume of a single landslide.

Figure 13b shows the statistical regression relationship between the landslide H_{max} and landslide volume. The relationship can be expressed as:

$$H_{max} = \frac{193.32 - 484.47}{1 + \left(\lg V_L / 1.05 \times 10^8 \right)^{1.13}} - 484.47$$

$$(R^2 = 0.32689) \tag{3}$$

Eq. 2 shows that the maximum runout of large-scale landslides in the study area exhibits a good correlation with landslide scale. This finding indicates that the larger the landslide, the larger the energy, leading to a longer runout.

The correlation coefficient between the landslide H_{max} and volume is small, and the correlation is relatively weak (Figure 13b and Eq. 3).

Figure 13c shows the statistical regression relationship between the landslide H_{max} and L_{max}. The relationship can be expressed as:

$$H_{max} = \frac{86.13 - 600.75}{1 + \left(L_{max} / 2279.39 \right)^{1.58}} - 600.75$$

$$(R^2 = 0.99) \tag{4}$$

Eq. 4 shows a good correlation between H_{max} of the large-scale landslides in the study area and their L_{max}.

The relationship between the runout and the vertical drop of the large-scale landslides in the study area is basically $L > 4H$. Most of the landslides triggered by the Wenchuan earthquake had $L = 4H$, whereas the landslides that occurred under normal gravity conditions had $L = 2H$. For the three types of
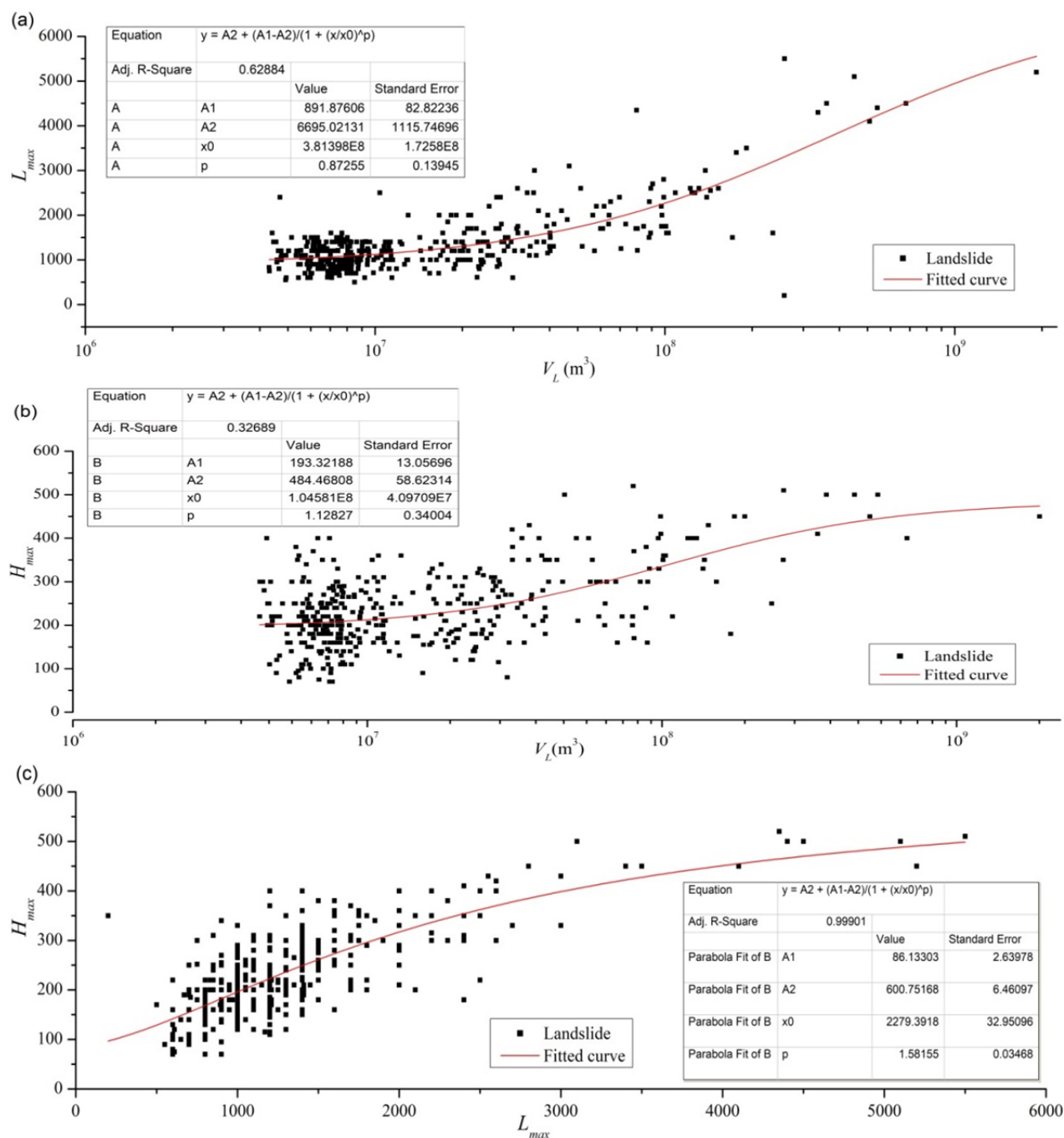

Figure 12 Landslide motion characteristic parameters.

Figure 13 Kinematic parameters relationship of large-scale landslide. (a) Logarithmic relationship diagram between landslide L_{max} and volume; (b) Logarithmic relationship diagram between landslide H_{max} and volume; (c) Relationship diagram between H_{max} and L_{max} for large-sized landslide (loess-mudstone plane/cutting landslide).

landslide (loess landslide, loess flow-slide and loess-mudstone interface landslide, Figure 6ABC), the relationship between height and length is nearly $L = 2H$. This result indicates strong mobility of large-scale landslides in the study area, suggesting powerful activity with devastating outcomes.

A database of geometrical measurements for individual landslides, including landslide area A_L (m²), and volume V_L (m³), was compiled by means of a worldwide literature search (Malamud et al. 2004; Guzzetti et al. 2009). Information on A_L and V_L was plotted in log–log coordinates for a total of 3856 landslides and 403 large-sized landslides
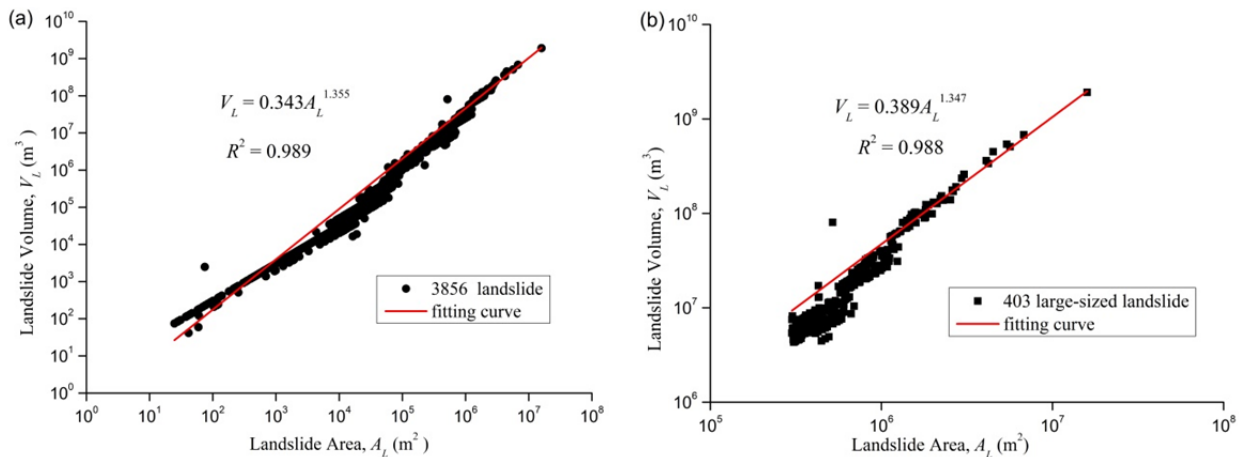
Figure 14 Empirical measurements for landslides in study area. Dots portray the area, A_L (x-axis, m²), and volume, V_L (y-axis, m³), of landslides. (a) the total 3856 landslides, and (b) the 403 large-sized landslides.

(Figure 14). Visual inspection of Figure 18 indicates a power-law equation (log–log coordinates) relationship between A_L and V_L, for multiple orders of magnitude, suggesting self-similar behavior of the dependency between landslide volume and area. For the relationship between A_L and V_L, the equation $V_L = aA_L^b$ was fitted to the empirical data. The empirical parameters are a = 0.07 - 0.087 and b = 1.292 - 1.45 (Guzzetti et al. 2009).

There is a linear (in log-log coordinates) relationship between A_L and V_L (Figure 14 a and b). In Figure 14a, A_L (x-axis) covers seven orders of magnitude ($2.5 \times 10^1 m^2 \leq A_L \leq 1.8 \times 10^7 m^2$) and V_L (y-axis) spans nine orders of magnitude ($4.2 \times 10^1 m^3 \leq V_L \leq 3.3 \times 10^9 m^3$). In the Figure 14b, A_L (x-axis) covers seven orders of magnitude ($2.5 \times 10^1 m^2 \leq A_L \leq 1.8 \times 10^7 m^2$) and V_L (y-axis) spans three orders of magnitude ($5.6 \times 10^5 m^3 \leq V_L \leq 3.3 \times 10^7 m^3$). The accuracy of each landslide measurement depends on the size of the landslide. This finding suggests self-similar behavior of the dependency between landslide area and volume (Guzzetti et al. 2009). In Figure 14 the scatter of the data around the tendency line is limited when the data are plotted in log coordinates.

Landslides frequency density can be expressed using the following equations (Malamud et al. 2004):

$$\int_0^\infty p\,(A_L)\,dA_L = 1 \qquad (5)$$

$$p\,(A_L) = \frac{1}{N_{LT}} \frac{\delta N_L}{\delta A_L} \qquad (6)$$

$$f\,(A_L) = \frac{\delta N_L}{\delta A_L} = N_{LT}\, p\,(A_L) \qquad (7)$$

where A_L is area of landslide, δN_L is the number of landslides with areas between A_L d $A_L + \delta A_L$, N_{LT} is the total number of landslides in an inventory, $p(A_L)$ is probability density function, and $f(A_L)$ is the frequency density of landslide areas.

Landslides frequency density area is plotted for a total of 3856 landslides in the study area (Figure 15a). Landslide frequency ranges from 3×10^3 to 4×10^5 km⁻² for landslide areas of 0.1 to 20 km². For landslide area of 1 to 7 km², landslide frequency is between 2×10^3 and 3×10^4 km⁻². Landslides are more intensive in this statistical range. The distribution map of landslide density in the study area is provided in Figure 15b. The districts with the highest landslide density are located in Tianshui city and Gangu town. The high-density area (index 11.4-15.96) is in the southern
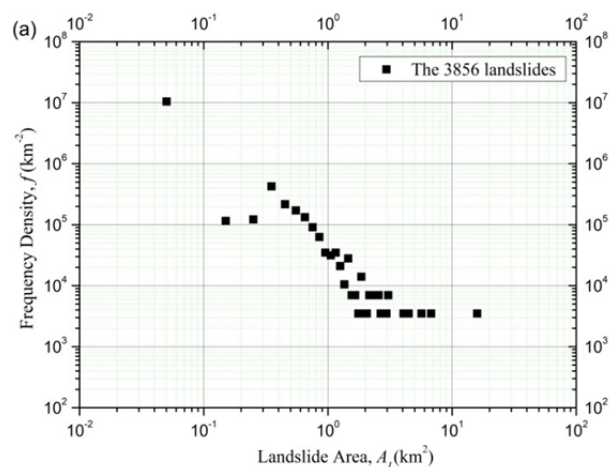

Figure 15 Landslides area relational graph (a) Dependence of the landslide frequency density f on landslide area A_L. (b) Landslide area density map. (-To be continued-)
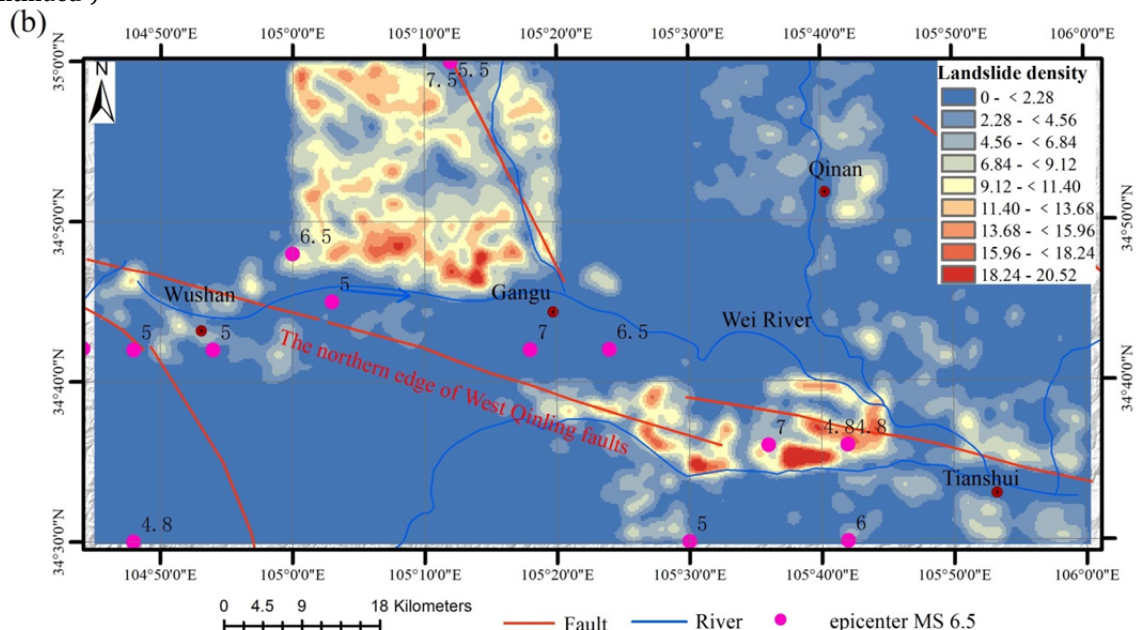
(-Continued-)

Figure 15 Landslides area relational graph (a) Dependence of the landslide frequency density *f* on landslide area A_L. (b) Landslide area density map.

part of Gangu town along the river, and a much higher-density area (index 15.96-20.52) is situated in the northwestern area of Tianshui city along the river.

The distance of the landslide movement is controlled by the total landslide energy, ignoring the effect of blockage of the landslide movement path. The landslide energy is equal to the product of the total slip mass and the vertical movement distance, where the slip mass is the product of the slip mass unit weight and the slip volume. Therefore, the landslide runout depends mainly on the landslide volume and the landslide vertical movement. Actual terrain is complex and includes rivers, buildings and protruding terrain. A landslide can result in the study area have not yet been investigated in detail. Accurate calculation of landslide volume from remote sensing images and DEM data is difficult, but the distribution area of landslides can be accurately obtained. Landslide thickness must be estimated based on experience, and this may lead to large errors.

In view of the uncertainty associated with the measurement of A_L and V_L, the landslides were of different morphological types and triggered by different causes, including rainfall and earthquakes. Our work on quantification of landslides is useful for estimating the role of landslides in assessing landslide hazards. Our work on the frequency–area

distribution of substantially landslide inventories also requires further testing. More high-quality, complete inventories are needed.

4 Discussion

In addition to earthquakes and heavy rain, river erosion also plays a role in the formation of landslides. When the slope toe of a landslide is eroded by downstream flow, a steep bank slope is formed. A strong earthquake can cause mountain slopes to slide and cover alluvial deposits. After long-term modification by geological erosion (weathering and erosion), the gradient of the front edge of the slope gradually diminishes and the slope stabilizes.

Field studies (Figure 1) show that the northern edge of the West Qinling fault zone is a sinistral active strike-slip fault, which has cut through the terraces, gullies and landslides in the study area during the Quaternary and is spreading in left row. The fault strike is 290°, and the tendencies are northeast and southeast. Ground motion was generated by the fault that triggerd large landslides near the fault zone perpendicular to the fault strike, within 5−10 km of both sides of the fault zone. Most of the large landslides have developed as a result of left-lateral motion of the fault, whereas

most of the landslides developed from right-lateral motion of the fault are small in size and volume. Strike-slip deformation produces mechanical effects such as extrusion, tension and shear slip, and some sections of the fault exhibit tensile properties. The fault activity is controlled by near-horizontal stress, whereas slope sliding is the result of gravity. The angle between the directions of these two stresses determines the effect of the sliding inertia force and controls the boundary and sliding direction of the landslide. Thus, the main sliding directions of the landslides in the fault region are southeast and southwest.

4.1 The shear zones

Shear zones in the mudstone are developed mostly in weak intercalated layers. Horizontal forces acting on the lamellar strata create curves and folds in rock, and coupling of forces form interlaminar shear zones. A shear zone can easily form when a rock mass contains hard and soft interbedded layers and a shear dislocation zone forms on the rock contact surface or inside a soft layer.

From the field investigation, we found that various types of shear zone are developed in the study area because of the different properties of the interlayers. Different boundary conditions and shear failure modes occur in these interlayers. The shear zones in the study area can be divided into several types (Figure 16).

Type (1): The shearing action is complete and the shear zone is well developed. Obvious tectonic dislocation and large shear displacement can be observed on the main shear plane. There are three forms of Type (1) shear zone.

(A) Complete shear–folding cleavage shear zone: this type of shear zone is developed along the primary claystone, with a wavy bedding pattern and cleavage around the shear zone. Clear tectonic zoning characteristics can be observed, such as an argillized zone, a sheared argillized surface, a cleavage folding zone and a joint zone (Figure 16A).

(B) Complete shear–shear fracture zone: this type shows interlaminar shear brittle fractures, and develops in the stratification of the medium-bedded mudstone. The weak intercalated layer in the mudstone is obvious, forming a continuous shear plane and exhibiting tectonic zoning. The

rock mass around the main shear plane has collapsed from shear failure with low-angle dip joints (Figure 16B).

(C) Complete shear–shear mixed zone: in this type, the mudstone interlayer has undergone shear fracturing in a random tectonic setting with disordered joints and a disorderly argillized layer. Such disturbed shear fracture zones are usually formed by strong seismic forces (Figure 16C).

Type (2): The shearing action is weak, and the shear zone is incomplete. The tectonic setting is weak and no obvious tectonic zones have formed. There are two forms of Type (2) shear zone.

(D) Incomplete shear–fracture shear zone: because of the boundary conditions and rock properties, a continuous, stable shear plane is not formed inside the interlayer. The shear displacement is not obvious and there are many joint fissures around the weak interlayer (Figure 16D).

(E) Incomplete shear–fissure tracing shear zone: this is a further development of (D). Under continuous shearing action, a wavy shear plane forms. Argillization can be observed locally, and tectonic zones are not obvious (Figure 16E).

Loess landslides, loess–mudstone interface landslides and loess flow-slides (Figure 6A, B, C) develop in the loess layer; for these landslide types, the different shear zones are not connected (Figure 16). In loess–mudstone plane/cutting landslides (Figure 6D, E), shear zones develop in the mudstone layer and the different types of shear zones are connected (Figure 16). Development of a shear zone will affect the movement characteristics of the landslide. A complete shear zone (Figure 16 A, B) affects the deformation mode of the landslide. The sliding surface of the landslide develops along the folding cleavage shear zone and the shear fracture zone. A zone of severe deformation (mixed shear zone; Figure 16C) is often found at the front part of a landslide. In an incomplete shear zone (Figure 16D, E) under deformation, the stress is not completely released. An incomplete shear zone usually develops into a loess–mudstone landslide.

4.2 The slip zone

In large-scale landslides the sliding zone often develops in the bedrock contact zone or in a weak interlayer of the mudstone and is almost horizontal.

As part of the field survey of the Miaoba landslide in the study area, boreholes were drilled and shear-wave velocity tests were conducted inside the borehole (Figure 17). The Miaoba landslide is a loess–mudstone cutting landslide (Figure 6E). The shear-wave velocity corresponds well with the hardness of the rock and soil. The shear-wave velocity of the rock and soil in the
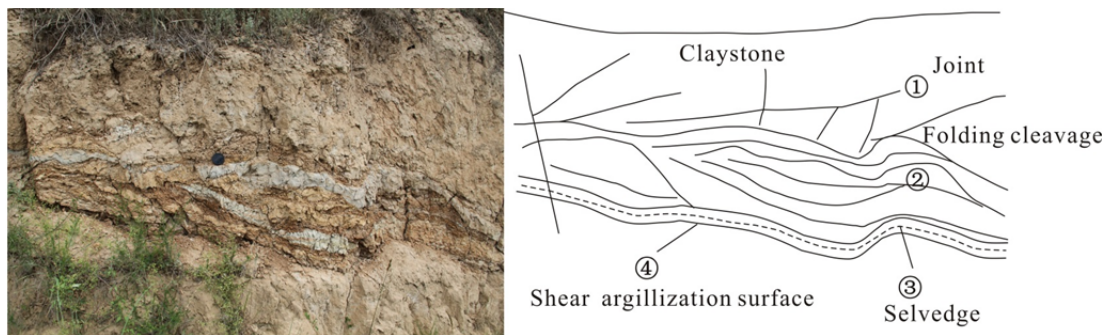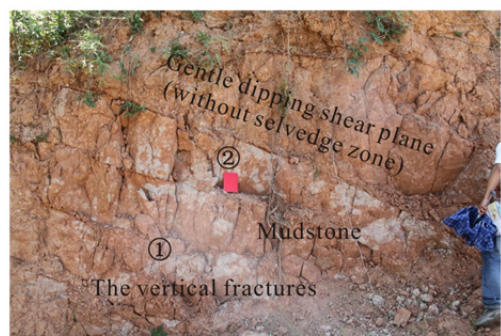

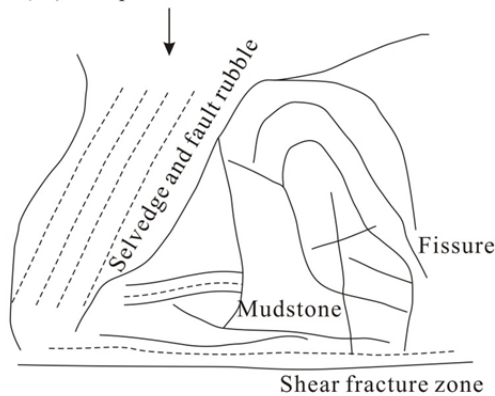(A) Complete shear - folding cleavage shear zone
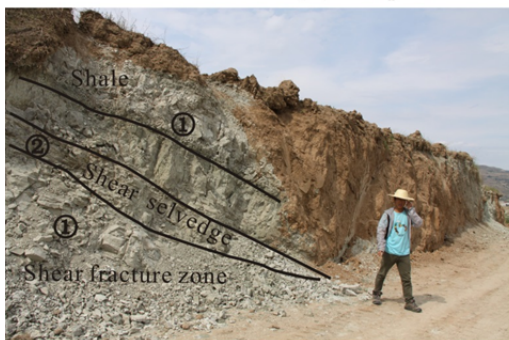
(B) Complete shear - shear fracture zone

(C) Complete shear - shear scrambled zone

(D) Incomplete shear - fissure shear zone

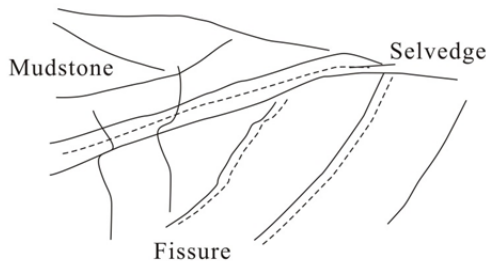(E) Incomplete shear - fissure tracking shear zone

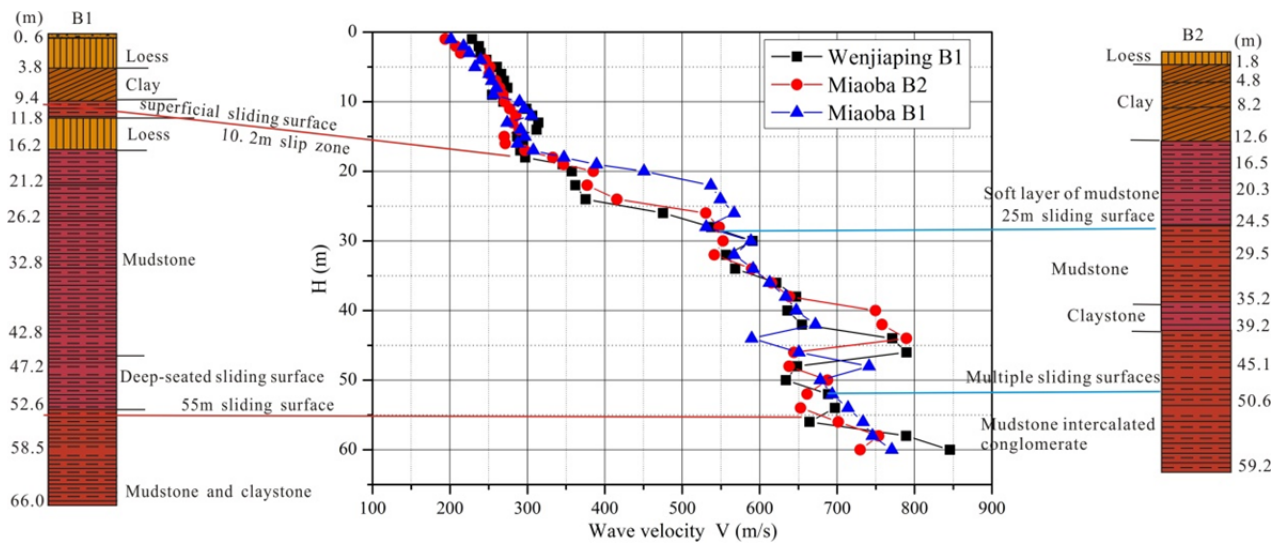**Figure 16** Shear zone characteristics in the study area.

Figure 17 Borehole log of large-scaled landslide (Wenjiaping village, Tianshui, 2015).
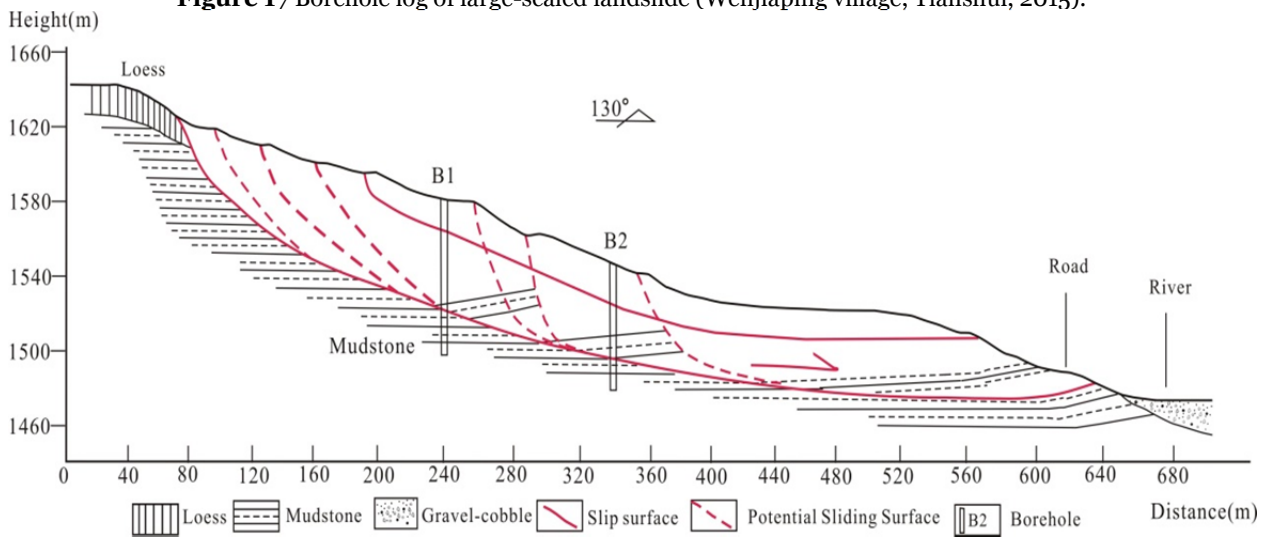

Figure 18 Geological profile of Miaoba landslide (Tianshui, 2015).

borehole increases with depth, reflecting the greater rock hardness with depth. The shear-wave velocity reveals the position of the sliding surface in the survey area. In the zone where the shear-wave velocity is abruptly reduced, the rock mass is weak, indicating the position of the shear surface. As shown in Figure 18, the shallow slip surface of the Miaoba landslide is located at depths of approximately 9.4–16.2 m, the mid-depth slip surface is at 25−35 m, and the deep slip surface is at 42.8–55 m.

Scanning electron microscope images of core samples from the Miaoba landslide are shown in Appendix 2. Images of undisturbed mudstone at magnifications of 500× and 2000× are shown in Appendix 2a and b, respectively. The undisturbed

mudstone (Appendix 2a and b) consists mainly of small aggregates with dispersed inter-aggregate pores. The undisturbed mudstone exhibits higher porosity, and the aggregates are in contact with neighboring particles via cementing bonds. The microscopic features show the development of Carnisaw soil structures with a flocculated pattern dominated by edge-to-face particle associations. There is no distinct structural anisotropy or preferential particle orientation in the undisturbed mudstone.

Images taken from the sliding surface are shown in Appendix 2c and d. Differences between the fabric of the undisturbed and sheared samples are evident. The clay fabric on the sliding surface exhibits a relatively uniform pore distribution,

whereas the particles in the undisturbed sample are grouped in connected assemblages. The sheared clay from the sliding surface has a more homogeneous structure than the undisturbed clay.

Linear striations are well developed on the shear surface, and the clay pores have a more uniform distribution than in the undisturbed clay because the shear sliding dissolves the clay aggregate, leading to smaller particle sizes. Thus, the clay microstructure aggregates become denser, indicating shearing–grinding activity.

5 Conclusions

We investigated the distribution and characteristics of loess landslides in Tianshui, Gansu Province, by means of field investigation, remote sensing interpretation and mapping. The landslides were classified on the basis of their failure mechanism. Analysis of landslide development and landslide classification based on the updated Varnes classification system and a literature review of landslide types in loess can improve our understanding of land failure types in the Tianshui region. The following conclusions were drawn.

1. A landslide database for the Tianshui region was established that contains information on landslide phenomena at different scales. The landslide distribution features were discussed. A total of 3856 landslides were investigated or interpreted from images. Landslides in the Tianshui Basin are mostly loess–mudstone landslides triggered by rainfall, construction work and earthquakes. The landslides mainly occur along the West Qinling faults on slopes with gradients of 10°–25° and on southeast- and southwest-facing slopes.

2. From the landslide database, 61.4% of the landslides are loess–mudstone plane or cutting landslides, 63.3% have volumes greater than 10^5 m³, and 68.4% are less than 10 m deep. On the basis of the landslide classification system of Varnes,

Hungr and a literature review of the landslide types in loess, these landslides were classified into five types on the basis of the features of their sliding surfaces: loess landslides, loess–mudstone interface landslides, loess flow-slides, loess–mudstone plane landslides and loess–mudstone cutting landslides. The evolution and failure process of each type of landslide was also discussed.

3. In the Tianshui area, shear zones in mudstone usually develop in weak intercalated layers. A number of shear failure modes were identified in the study area, which were classified into two groups of shear zones—complete and incomplete. These groups were further divided into five types: complete shear–folding cleavage shear zone; complete shear–shear fracture zone; complete shear–shear mixed zone; incomplete shear–fracture shear zone and incomplete shear–fissure tracing shear zone.

4. The formation mechanism and motion characteristics of large-scale landslides were analyzed. Most of the landslides had a gentle slope, long runout and high risk. The relationship between the runout L and the vertical drop H of the large-scale landslides in the study area was generally $L > 4H$. The relationship between landslide area and volume was also addressed. The relationship $V_L = aA_L^b$ was fitted to the empirical data. The relationship between landslide area and frequency was also discussed. High-frequency zones of landslide distribution in the study area were delineated. The sliding zones of large-scale landslides are often developed in the bedrock contact zone or in the weak interlayer of the mudstone and are almost horizontal. Microstructure analysis showed that the undisturbed mudstone consists mainly of small aggregates with dispersed inter-aggregate pores. The sheared clay has a more homogeneous structure than the undisturbed clay. Linear striations are well developed on the shear surface, and the clay pores have a more uniform distribution than in the undisturbed clay.

Electronic supplementary material: Supplementary material (Appendixes 1,2) are available in the online version of this article at https://doi.org/10.1007/s11629-019-5595-4

References

China Seismological Bureau (1980) Gansu Earthquake. China Earthquake Administration Lanzhou Institute of Seismology, Lanzhou. (In Chinese).

Chen Y, Shi Y, Liu H, et al. (2005) Analysis of Distribution Characteristics and Influencing Factors of Earthquake Landslides in Loess Area. Earthquake Research in China 21(2):235-243. (In Chinese)

Crandell DR, Miller CD, Glicken HX, et al. (1984) Catastrophic debris avalanche from ancestral Mount Shasta volcano, California. Geology 12 (3): 143-146. https://doi.org/10.1130/0091-7613(1984)12<143:CDAFAM>2.0.CO;2

Crozier MJ (2010). Landslide geomorphology: An argument for recognition, with examples from New Zealand. Geomorphology 120: 3-15. https://doi:10.1016/j.geomorph.2009.09.010

Derbyshire E (2001) Geological hazards in loess terrain, with particular reference to the loess regions of china. Earth-Science Reviews 54(1): 231-260. https://doi.org/10.1016/S0012-8252(01)00050-2

Duman TY, Çan T, Emre Ö, et al. (2005) Landslide inventory of northwestern Anatolia, Turkey. Engineering Geology 77(1-2): 99-114. https://doi.org/10.1016/j.enggeo.2004.08.005

Da P, Shun Y, Xiaobo LI, et al. (2017) Distribution and mechanism of loess landslides induced by earthquake in Tongwei, Gansu Province. Chinese Journal of Geological Hazard & Control 29(3): 31-38. (In Chinese)

Evans SG, Hungr O, Clague JJ (2001) Dynamics of the 1984 rock avalanche and associated distal debris flow on Mount Cayley, British Columbia, Canada; implications for landslide hazard assessment on dissected volcanoes. Engineering Geology 61(1): 29-51. https://doi.org/10.1016/S0013-7952(00)00118-6

Fan X, Tian S, Duan X, et al. (2014) Study of topography factors influence on motion parameters for seismic slope-toe landslides. Chinese Journal of Rock Mechanics and Engineering 33(s2): 4056-4066. (In Chinese)

Hungr O, Evans SG, Bovis MJ, et al. (2011) A review of the classification of landslides of the flow type. environmental & engineering geoscience 7 (3): 221-238. https://doi.org/10.2113/gseegeosci.7.3.221

Harp EL, Jibson RW (1996) Landslides triggered by the 1994 Northridge, California, earthquake. Bulletin of the seismological society of America 86 (1B):319-332. https://pubs.geoscienceworld.org/ssa/bssa/article-abstract/86/1B/S319/120090/landslides-triggered-by-the-1994-northridge

Huang H, Song K, Yi W, et al. (2019) Use of multi-source remote sensing images to describe the sudden Shanshucao landslide in the three gorges reservoir, China. Bulletin of Engineering Geology and the Environment 78: 2591-2610. https://doi.org/10.1007/s10064-018-1261-2

Han Z J, Xiang H F, Guo S M (2001) Preliminary study on active features of Fenghuangshan-Tianshui fault, west Qinling north boundary fault zone since the late of late Pleistocene. Acta Seismologica Sinica 14(2): 230-233. https://doi.org/10.1007/s11589-001-0153-9

Guzzetti F, Ardizzone F, Cardinali M, et al. (2009) Landslide volumes and landslide mobilization rates in Umbria, central Italy. Earth and Planetary Science Letters 279: 222–229. https://doi:10.1016/j.epsl.2009.01.005

Li C, Zhang PZ, Yin J, et al. (2009) Late Quaternary left-lateral slip rate of the Haiyuan fault, northeastern margin of the Tibetan Plateau. Tectonics 28 (5): TC5010. https://doi:10.1029/2008TC002302

Lin ML, Tung CC (2004) A GIS-based potential analysis of the landslides induced by the Chi-Chi earthquake. Engineering Geology 71(1): 63-77. https://doi.org/10.1016/S0013-7952(03)00126-1

Li C, Su H, Zhang H, et al. (2016) Correlation between the spatial distribution of radon anomalies and fault activity in the northern margin of West Qinling Fault Zone, Central China. Journal of Radioanalytical and Nuclear Chemistry 308(2): 679-686. https://doi.org/10.1007/s10967-015-4504-8

Liu Y, Gao A, Shi J, et al. (2007) Prilimary result of temperature distribution and associated thermal stress in crust in Tianshui, China. Acta Seismol. Sin. (Engl. Ed.) 20(6): 641-655. https://doi:10.1007/s11589-007-0641-7

Meng XM, Zhang SW (1989) Investigation of dangerous loess slopes in the Lanzhou region. Internal Report, Geological Hazards Research Institute, Lanzhou, 89 pp. (In Chinese)

Meng XM, Derbyshire E (1998) Landslides and their control in the Chinese Loess Plateau models and case studies from Gansu Province, China. Geological Society, London, Engineering Geology Special Publications 15(1): 141-153. https://doi.org/10.1144/GSL.ENG.1998.015.01.15

Malamud BD, Turcotte DL, Guzzetti F, et al. (2004) Landslides, earthquakes, and erosion. Earth and Planetary Science Letters 229(1-2): 0-59. https://doi.org/10.1016/j.epsl.2004.10.018

Malamud BD, Turcotte DL, Guzzetti F, et al. (2004) Landslide inventories and their statistical properties. Earth Surface Processes and Landforms 29: 687-711. https://doi:10.1002/esp.1064

Owen LA, Kamp U, Khattak GA, et al. (2008) Landslides triggered by the 8 October 2005 Kashmir earthquake. Geomorphology 94 (1): 1-9. https://doi.org/10.1016/j.geomorph.2007.04.007

Peng J, Ma P, Wang Q, et al. (2018) Interaction between landsliding materials and the underlying erodible bed in a loess flowslide. Engineering Geology 234: 38-49. https://doi.org/10.1016/j.enggeo.2018.01.001

Peng X, Zhen L, Shu-Ren W, et al. (2018) Rotational–translational landslides in the neogene basins at the northeast margin of the Tibetan Plateau. Engineering Geology 244: 107-115. https://doi.org/10.1016/j.enggeo.2018.07.024

Peng J, Fan Z, Wu D, et al. (2015) Heavy rainfall triggered loess–mudstone landslide and subsequent debris flow in Tianshui, China. Engineering Geology 186: 79-90. https://doi.org/10.1016/j.enggeo.2014.08.015

Peng D, Xu Q, Liu F, et al. (2018) Distribution and failure modes of the landslides in Heitai terrace, China. Engineering Geology 236: 97-110. https://doi.org/10.1016/j.enggeo.2017.09.016

Parker RN, Densmore AL, Rosser NJ, et al. (2011) Mass wasting triggered by the 2008 Wenchuan earthquake is greater than orogenic growth. Nature Geoscience 4(7): 449-452. https://doi.org/10.1038/ngeo1154

Qu C, Zuo R, Shan X, et al. (2017) Coseismic deformation of the

2016 Taiwan Mw6.3 earthquake using InSAR data and source slip inversion. Journal of Asian Earth Sciences 148:96-104. https://doi.org/10.1016/j.jseaes.2017.08.027

Rosi A, Tofani V, Tanteri L, et al. (2017) The new landslide inventory of Tuscany (Italy) updated with PS-InSAR: geomorphological features and landslide distribution. Landslides 15(1): 5-19. https://doi.org/10.1007/s10346-017-0861-4

Seismological Institute of Lanzhou, SSB and Seismological Team of Ningxia Hui Autonomous Region (1980) Haiyuan Great Earthquake in 1920. Seismological Press, Beijing. (In Chinese)

Sun P, Li RJ, Jiang H, et al. (2017) Earthquake-triggered landslides by the 1718 Tongwei earthquake in Gansu Province, northwest China. Bulletin of Engineering Geology and the Environment 76: 1281-1295. https://doi.org/10.1007/s10064-016-0949-4

Sato HP, Harp EL (2009) Interpretation of earthquake-induced landslides triggered by the 12 May 2008, M7.9 Wenchuan earthquake in the Beichuan area, Sichuan Province, China using satellite imagery and Google Earth. Landslides 6: 153-159. https://doi.org/10.1007/s10346-009-0147-6

Spreafico MC, Wolter A, Picotti V, et al. (2018) Forensic investigations of the Cima Salti landslide, northern Italy, using runout simulations. Geomorphology 318:172-186. https://doi.org/10.1016/j.geomorph.2018.04.013

Sato HP, Hasegawa H, Fujiwara S, et al. (2007) Interpretation of landslide distribution triggered by the 2005 northern Pakistan earthquake using Spot 5 imagery. Landslides 4(2): 113-122. https://doi.org/10.1007/s10346-006-0069-5

Varnes DJ (1978) Slopemovement Types and Processes. In: Schuster RL and Krizek RJ Eds, Special Report 176: Landslides: Analysis and Control Transportation and Road Research Board, National Academy of Science, Washington DC. Pp 11-33.

Van Westen CJ, Van Asch TWJ, Soeters R (2006) Landslide hazard and risk zonation —why is it still so difficult? Bulletin of Engineering Geology and the Environment 65: 167-184. https://doi.org/10.1007/s10064-005-0023-0

Wu W, Wang N (2006) Landslides in Gansu Province. Lanzhou University Press, Lanzhou. pp 88-97. (In Chinese)

Wang FW, Sassa Kyoji, Wang G (2002) Mechanism of a long-runout landslide triggered by the August 1998 heavy rainfall in Fukushima Prefecture, Japan. Engineering Geology 63(1): 169-185. https://doi.org/10.1016/S0013-7952(01)00080-1

Wang T, Wu S, Shi J, et al. (2018) Assessment of the effects of historical strong earthquakes on large-scale landslide groupings in the Wei River midstream. Engineering Geology 235: 11-19. https://doi.org/10.1016/j.enggeo.2018.01.020

Yang X, Chen L (2010) Using multi-temporal remote sensor imagery to detect earthquake-triggered landslides. International Journal of Applied Earth Observation and Geoinformation 12(6): 487-495. https://doi.org/10.1016/j.jag.2010.05.006

Zhuang J, Peng J, Xu C, et al. (2018) Distribution and characteristics of loess landslides triggered by the 1920 Haiyuan Earthquake, Northwest of China. Geomorphology 314: 1-12. https://doi.org/10.1016/j.geomorph.2018.04.012

Zhang F, Wang G (2018) Effect of irrigation-induced densification on the post-failure behavior of loess flowslides occurring on the Heifangtai area, Gansu, China. Engineering Geology 236: 111-118. https://doi.org/10.1016/j.enggeo.2017.07.010

Zhang SL, Zhu ZH, Qi SC, et al. (2018) Deformation process and mechanism analyses for a planar sliding in the Mayanpo massive bedding rock slope at the Xiangjiaba Hydropower Station. Landslides 15: 2061-2073. https://doi.org/10.1007/s10346-018-1041-x